

NACA RM L53110



# RESEARCH MEMORANDUM

FLIGHT TEST RESULTS OF ROCKET-PROPELLED BUFFET-RESEARCH  
MODELS HAVING 45° SWEEPBACK WINGS AND 45° SWEEPBACK  
TAILS LOCATED IN THE WING CHORD PLANE

By Homer P. Mason

Langley Aeronautical Laboratory  
Langley Field, Va.

**CLASSIFICATION CANCELLED**

Authority: *Lang. Res. Rep. 4* Date *9-24-56*  
*RN-107*  
By: *H.P.M.* 10-8-56 See

CLASSIFIED DOCUMENT

This material contains information affecting the National Defense of the United States within the meaning of the espionage laws, Title 18, U.S.C., Secs. 793 and 794, the transmission or revelation of which in any manner to an unauthorized person is prohibited by law.

## NATIONAL ADVISORY COMMITTEE FOR AERONAUTICS

WASHINGTON

November 4, 1953

## NATIONAL ADVISORY COMMITTEE FOR AERONAUTICS

## RESEARCH MEMORANDUM

FLIGHT TEST RESULTS OF ROCKET-PROPELLED BUFFET-RESEARCH  
MODELS HAVING  $45^\circ$  SWEEPBACK WINGS AND  $45^\circ$  SWEEPBACK  
TAILS LOCATED IN THE WING CHORD PLANE

By Homer P. Mason

## SUMMARY

Three rocket-propelled buffet-research models have been flight tested to determine the buffeting characteristics of a swept-wing-airplane configuration with the horizontal tail operating near the wing wake. The models consisted of parabolic bodies having  $45^\circ$  sweptback wings of aspect ratio 3.56, a taper ratio of 0.3, NACA 64A007 airfoil sections, and tail surfaces of geometry and section identical to the wings. Two tests were conducted with the horizontal tail located in the wing chord plane with fixed incidence angles of  $-1.5^\circ$  on one model and  $0^\circ$  on the other model. The third test was conducted with no horizontal tail.

Results of these tests are presented as incremental accelerations in the body due to buffeting, trim angles of attack, trim normal- and side-force coefficients, wing-tip helix angles, static-directional-stability derivatives, and drag coefficients plotted against Mach number. These data indicate that mild low-lift buffeting was experienced by all models over a range of Mach number from approximately 0.7 to 1.4. It is further indicated that this buffeting was probably induced by wing-body interference and was amplified at transonic speeds by the horizontal tail operating in the wing wake. A longitudinal trim change was encountered by the tail-on models at transonic speeds, but no large changes in side force and no wing dropping were indicated.

## INTRODUCTION

Recent designs for high-speed airplanes incorporate very low horizontal-tail positions. Since tail surfaces located near the wing chord plane operate in or very near the wing wake at low angles of attack, a knowledge of the effects of wing wake on tail buffeting at transonic

speeds has become important. The tests reported herein were conducted to determine the low-lift buffeting characteristics of an airplane configuration having a  $45^\circ$  sweptback tail located in the chord plane of a  $45^\circ$  sweptback wing.

## SYMBOLS

A	cross-sectional area, sq ft
$\Delta a_n$	increment of normal acceleration due to buffeting (both positive and negative about mean line), g units
$\Delta a_t$	increment of transverse acceleration due to buffeting, g units
b	wing span, ft
$\bar{c}$	mean aerodynamic chord of wing, 1.348 ft
$I_z$	moment of inertia about Z-axis, approximately 8.1 slug-ft <sup>2</sup>
$i_t$	horizontal-tail incidence, deg
L	length of body, ft
M	Mach number
$P_z$	period of yawing oscillation, sec
p	rolling velocity, radians/sec
$pb/2V$	wing-tip helix angle, radians
q	dynamic pressure, lb/sq ft
R	Reynolds number based on wing $\bar{c}$
S	total wing area, 5.38 sq ft
V	velocity, fps
$\alpha$	angle of attack, deg
$C_D$	drag coefficient, Drag/qS

$C_N$	normal-force coefficient, $\frac{\text{Normal force}}{qS}$
$C_Y$	side-force coefficient, $\frac{\text{Side force}}{qS}$
$C_{N_\alpha}$	normal-force-curve slope per degree
$C_{n_\beta}$	static-directional-stability derivative, approximately $-\frac{4\pi^2 I_Z}{57.3 q S b P_Z^2}$
$h_1$	altitude range, 2,000 to 9,000 ft
$h_2$	altitude range, 10,000 to 20,000 ft

#### MODELS

Principal dimensions and geometric characteristics of the test models are shown in figure 1. The longitudinal distribution of cross-sectional area is shown in figure 2. A photograph of a complete configuration is shown in figure 3, and a photograph of a model-booster combination on the launcher is shown in figure 4. The fuselage used for these tests was the basic body used in the tests presented in reference 1. Wing and tail surfaces were of aspect ratio 3.56, taper ratio 0.3, NACA 64A007 airfoil section, and had  $45^\circ$  sweepback of the quarter-chord line. All surfaces were constructed of laminated spruce with aluminum-alloy surface inlays.

Three models were tested which differed externally only in the horizontal tail, one model having no horizontal tail, one model having  $i_t = 0^\circ$ , and one model having  $i_t = -1.5^\circ$  (trailing edge up). The two models having horizontal tails had internal sustainer-rocket motors with nozzles machined to provide  $-2^\circ$  thrust inclination relative to the model center line to obtain positive trim angles of attack during sustainer burning. The tail-off model, which had a sustainer with no intentional thrust inclination, weighed approximately 117 pounds during the low-altitude flight range and approximately 106 pounds during the high-altitude flight range. The model with  $i_t = 0^\circ$  weighed approximately 98 pounds, and the model with  $i_t = -1.5^\circ$  weighed approximately 101 pounds.

## INSTRUMENTATION

Instrumentation common to all models was as follows: a normal and a transverse accelerometer in the body near the tail-root quarter chord, a normal and a longitudinal accelerometer near the wing-root quarter chord, and a standard NACA vane-type angle-of-attack indicator sting-mounted ahead of the nose. Transverse accelerometers were installed near the wing-root quarter chord on the tail-off model and the model with  $i_t = 0^\circ$ . A rocket-chamber pressure pickup for use in determining sustainer-rocket thrust was incorporated in the model having  $i_t = -1.5^\circ$ . All normal and transverse accelerometers had natural frequencies of the order of 75 to 100 cps and 50 to 70 percent critical damping.

## TESTS

## Ground Tests

Static firing tests of one sustainer-rocket motor were conducted to determine the thrust and the approximate contribution of the thrust to the normal acceleration due to the inclined thrust axis.

Shake tests of each model were conducted to determine natural frequencies and modes of vibration. The results of these tests are presented in table I. The intermediate wing frequencies were recorded by the accelerometers in shake tests of all models but the mode shape was identified only on the tail-off model.

## Flight Tests

Models having horizontal tails were accelerated rapidly to approximately  $M = 0.85$  by external booster-rocket motors, and after booster separation were accelerated to approximately  $M = 1.4$  by the internal sustainer-rocket motors. The tail-off model was accelerated to approximately  $M = 1.5$  by a 6-inch ABL Deacon rocket motor and was then allowed to coast to approximately  $M = 0.9$  before the sustainer rocket fired and accelerated the model to approximately  $M = 1.4$ . Only the data from the coasting portions of this flight are presented, and, where applicable, the proper altitude ranges for each coast period are indicated by the symbols  $h_1$  and  $h_2$ . Accelerations, angle of attack, and, in one case, rocket-chamber pressure were transmitted to the ground and recorded by using the standard NACA telemetering system. Velocities were obtained by using a CW Doppler radar set, flight-path data by using NACA modified SCR 584 tracking radar, and rolling velocity by using a spinsonde recorder

and the telemeter antenna. Atmospheric data were obtained from radiosondes released either just before or just after each flight. These tests were conducted at the Langley Pilotless Aircraft Research Station at Wallops Island, Va. The scale of these tests is shown in figure 5 as the variation of Reynolds number, based on the wing mean aerodynamic chord of 1.348 feet, with Mach number for the coasting portions of each flight. The variation of free-stream dynamic pressure with Mach number for each flight is shown in figure 6.

### Accuracy

The maximum probable systematic errors in absolute values of  $\alpha$ ,  $C_N$ ,  $C_Y$ , and  $C_D$  due to instrument calibration ranges are summarized as follows:

	M = 0.8	M = 1.2
$\alpha$ , deg . . . . .	$\pm 0.5$	$\pm 0.5$
$C_N$ . . . . .	$\pm 0.02$	$\pm 0.01$
$C_Y$ . . . . .	$\pm 0.02$	$\pm 0.01$
$C_D$ . . . . .	$\pm 0.01$	$\pm 0.005$

Based on the width of the recorded accelerometer traces and the calibration data for the individual instruments, it is estimated that the average minimum buffet amplitude which could be identified in these tests was approximately  $\pm 0.05g$ . Mach numbers are estimated to be accurate within approximately 1 percent at supersonic speeds and 2 percent at subsonic speeds. Some unidentified vibrations were recorded below this level but have not been considered to be buffeting in the analysis of these tests. The values of  $\Delta g$  due to buffeting presented herein are the measured values of  $\Delta g$  corrected by amplitude response factors ranging from extremes of 0.5 to 1.1 in accordance with the buffet frequencies encountered and the damping characteristics of the individual accelerometer-recorder systems. Values of  $\Delta g$  due to buffeting have not been corrected for differences in model weights.

### RESULTS AND DISCUSSION

Results obtained from flight tests of two buffet-research models having  $45^\circ$  sweptback tail surfaces located in the chord plane of  $45^\circ$  sweptback wings are presented herein for a Mach number range from approximately 0.7 to 1.4 and are compared with results from tests of a similar

model having no horizontal tail. The expressions "tail on" and "tail off" as used herein refer only to the horizontal-tail surfaces. All coefficients are based on the total wing area and wing span.

#### Trim

The trim characteristics of each model are shown in figures 7 to 10 as the variation of angle of attack  $\alpha$ , normal-force coefficient  $C_N$ , side-force coefficient  $C_Y$ , and wing-tip helix angle  $\phi_b/2V$  with Mach number. Trim  $\alpha$  and trim  $C_N$  are shown for both power-on and power-off flight for the tail-on models to show the effects of the inclined thrust axis. Longitudinal trim characteristics of the tail-off model were almost identical for both coasting portions of flight; hence, only one trim curve is shown. Both tail-on models experienced longitudinal trim changes as the Mach number increased from approximately 0.94 to 0.98 (figs. 7 and 8), but no transonic trim changes were experienced by the tail-off model.

Trim side-force coefficients, figure 9, indicate that no large lateral trim changes were encountered by either of the models tested although addition of the horizontal tail appears to have produced some small irregularities in  $C_Y$  between Mach numbers of approximately 0.95 and 1.0. Wing-tip helix angles, figure 10, indicate that no wing drooping was experienced by any of the models tested.

#### Buffeting

Short portions of the telemeter records of normal accelerations for the tail-off model and the model having  $i_t = 0^\circ$  are shown in figure 11 to illustrate the random character of the buffet oscillations recorded in these tests. Buffeting was encountered by all models at trim conditions in both power-on and power-off flight over the complete test Mach number range from approximately 0.7 to 1.4. Power-on buffet intensities, however, are not presented because the contribution of the sustainer-rocket-motor shaking to the recorded amplitudes is not known. Buffet intensities measured in both the normal and transverse planes during coasting flight are presented in figures 12 and 13 as the increment of acceleration due to buffeting, corrected for amplitude response, plotted against Mach number. Buffet intensities are shown as values of  $\Delta g$  rather than as coefficients because of the difficulty of relating them to any one surface. Random vibrations were recorded for all models between Mach numbers of approximately 0.6 and 0.7, but are not presented because the amplitudes were of the same order of magnitude as the estimated minimum intensity which could be identified as buffeting.

The buffeting, indicated by the accelerometer near the wing root, which was encountered by the tail-off model at transonic speeds was only about half the magnitude of  $\Delta a_n$  measured on the tail-on models. At supersonic speeds, the buffeting encountered by the tail-off model and the tail-on model with  $i_t = 0^\circ$  was of about the same magnitude. The buffet data obtained at supersonic speeds for the model having  $i_t = -1.5^\circ$  is believed insufficient for adequate comparison or analysis. Buffet frequencies experienced by all models corresponded to structural frequencies of the models, but the intermediate wing bending frequency was predominant.

The buffeting encountered in these tests is considered very mild since the wing loading of the models was only about 20 lb/sq ft. However, at lift coefficients required for effective operation of a full-scale airplane, these intensities might be multiplied several times. The estimated value of  $C_{N_\alpha}$  for these models is approximately 0.055 at  $M = 1.4$  and 0.08 at  $M = 0.8$ .

Little significance is placed on the buffet intensities recorded in the transverse plane, figure 13, because it is not known whether these vibrations were due to aerodynamically induced loads in this plane or to structural vibrations induced by buffeting in the normal plane.

The buffet intensity at transonic speeds, as indicated by the wing-root accelerometers, was increased appreciably by the presence of the horizontal tail (fig. 12). Since buffeting occurred on the tail-off model, it appears that the primary buffeting occurred ahead of the tail surfaces and was amplified by the tail operating in the wing wake at transonic speeds.

Data from references 1 and 2 indicate that 7-percent-thick surfaces swept back  $45^\circ$  probably would not experience low-lift buffeting. Reference 3 indicates that even much thicker surfaces should not experience low-lift buffeting above approximately  $M = 1.0$ . Thus, it is believed unlikely that the buffeting encountered in the present tests was due only to thickness of the lifting surfaces.

Reference 4 shows pressure pulsations, believed to be indications of buffeting, on a two-dimensional NACA 64A006 airfoil section at low lift coefficients from approximately  $M = 0.5$  to the test limit near  $M = 1.0$ . These pulsations were more severe and covered a wider Mach number range than similar pulsations on an NACA 65A006 airfoil section. Thus, it appears that the 64A-series airfoil sections used in the present tests may have worse buffeting characteristics than the 65A-series airfoil sections of the free-flight tests of references 1 to 3. Although it does not seem probable that low-lift buffeting due to section characteristics would extend much above  $M = 1.0$  (refs. 1, 3, and 4), it cannot be definitely stated at this time that the buffeting encountered in the present tests was not due to airfoil-section characteristics.

As previously stated, the predominant buffet frequency encountered by all models corresponds to the intermediate wing bending frequency. This frequency, see table I, represents a mode of vibration in which the only node lines are located outboard of the 0.5 wing semispan and the body is at the position of maximum wing deflections. Thus, small forces on or near the body or on the wing tip could readily excite vibrations in this mode, and accelerometers in the body would measure the accelerations resulting from the vertical movement of the body. Ordinarily, when buffeting is induced by airfoil-section characteristics, the region of separated flow over the surface is fairly extensive and excites a first bending structural mode. The fact that this intermediate mode was excited indicates that the disturbance was probably on or near the wing-body juncture. It is thought that an interference separation phenomenon may exist in this region as a result of the maximum thickness of the wing root lying very close to the maximum body diameter.

It is believed, therefore, that the buffeting encountered in the present tests was probably caused by interference at the wing-body juncture, and that this buffeting was amplified at transonic speeds by the horizontal tail operating in the wing wake. Data from these tests, however, are insufficient to determine the characteristics of a tail operating in the wake of an aerodynamically clean wing-body combination.

#### Unidentified Vibration

An extremely large amplitude vibration of regular nature occurred during supersonic coasting flight of the model having  $i_t = -1.5^\circ$  at frequencies which varied from approximately 170 cps at  $M = 1.4$  to approximately 140 cps at  $M = 1.0$ . This vibration was recorded by both normal accelerometers and by the angle-of-attack indicator, but has not been identified and did not occur on either of the other two similar models. Note, however, that this model had a considerably lower wing-second-bending frequency than either of the other models, table I. It is felt that the large amplitude vibration experienced in this test was some nondestructive flutter mode.

#### Static Directional Stability

Static-directional-stability derivatives  $C_{n\beta}$  were calculated from random small yawing oscillations of the test models and are plotted against Mach number in figure 14. A decrease in stability with Mach number at supersonic speeds is indicated.

~~CONFIDENTIAL~~

## Drag

Total drag coefficients for the tail-off model and for the model having  $i_t = 0^\circ$  are plotted in figure 15 against Mach number. Also shown for comparison is the drag-coefficient curve for the basic body alone as estimated from the data of reference 5. It may be seen that the addition of the wings of the present tests to the basic body reduced the drag-rise Mach number approximately 0.05. Supersonic drag coefficients for the tail-on model were approximately 10 percent greater than those for the tail-off model.

The longitudinal distribution of cross-sectional area of these models is shown nondimensionally in figure 2 as the area at a given station divided by the square of the body length plotted against body station. It is of interest to note that the ratio of the drag rise with tail off to the drag rise with tail on is almost identical to the ratio of the maximum value of  $A/L^2$  at the tail.

## CONCLUDING REMARKS

Flight tests have been made of two rocket-propelled buffet-research models having  $45^\circ$  sweptback tail surfaces mounted on parabolic bodies in the chord plane of  $45^\circ$  sweptback wings and of one similar model with no horizontal-tail surfaces. The results indicate that low-lift buffeting was induced over a wide range of subsonic, transonic, and supersonic Mach numbers, probably as a result of wing-body interference when the wing maximum thickness was located near the maximum body diameter. This buffeting was apparently amplified at transonic speeds by the horizontal tail operating in the wing wake. A longitudinal trim change was experienced by the tail-on models at transonic speeds, but no large lateral trim changes and no wing dropping were indicated.

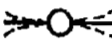
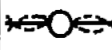
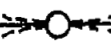
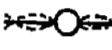
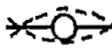
Langley Aeronautical Laboratory,  
National Advisory Committee for Aeronautics,  
Langley Field, Va., August 26, 1953.

## REFERENCES

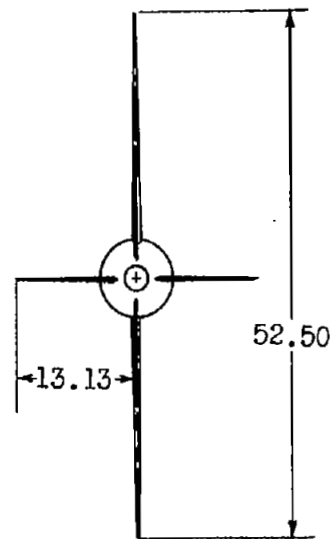
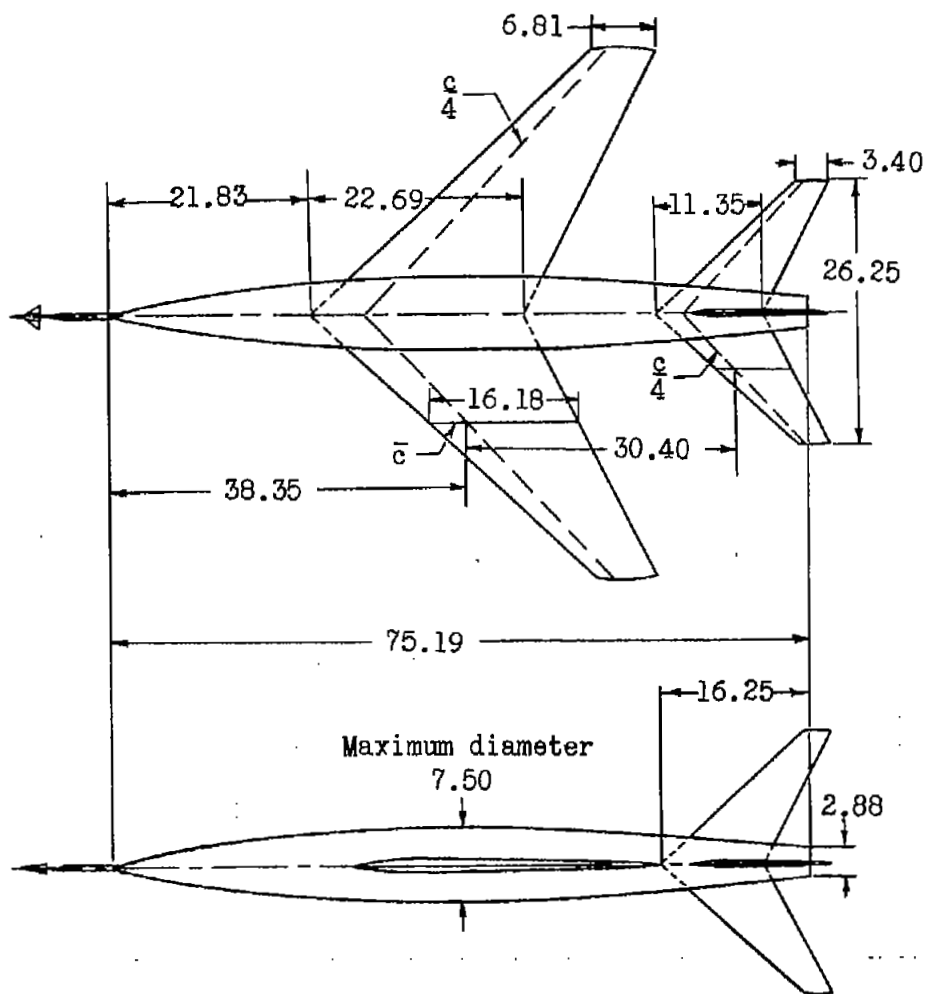
1. Mason, Homer P., and Gardner, William N.: An Application of the Rocket-Propelled-Model Technique to the Investigation of Low-Lift Buffeting and the Results of Preliminary Tests. NACA RM L52C27, 1952.
2. Purser, Paul E.: Notes on Low-Lift Buffeting and Wing Dropping at Mach Numbers Near 1. NACA RM L51A30, 1951.
3. Mason, Homer P.: Low-Lift Buffet Characteristics Obtained From Flight Tests of Unswept Thin Intersecting Surfaces and of Thick 35° Swept-back Surfaces. NACA RM L52H12, 1953.
4. Humphreys, Milton D., and Kent, John D.: The Effects of Camber and Leading-Edge-Flap Deflection on the Pressure Pulsations on Thin Rigid Airfoils at Transonic Speeds. NACA RM L52G22, 1952.
5. Hart, Roger G., and Katz, Ellis R.: Flight Investigations at High-Subsonic, Transonic, and Supersonic Speeds To Determine Zero-Lift Drag of Fin-Stabilized Bodies of Revolution Having Fineness Ratios of 12.5, 8.91, and 6.04 and Varying Positions of Maximum Diameter. NACA RM L9I30, 1949.

TABLE I  
 NATURAL FREQUENCIES AND MODE SHAPES OF MODELS

[Ground-shake test results]

Model	First wing bending, cps	Second wing bending, cps	Wing torsion, cps	First tail bending, cps	Second tail bending, cps	Intermediate wing bending, cps
						
Tail off . . . . .	62	222	316			90 to 120
$i_t = 0^\circ$ . . . . .	62	210	300	126	195	94 to 112
$i_t = -1.5^\circ$ . . . . .	62	143	305	135	250	92 to 115





All surfaces:  
 Aspect ratio.....3.56  
 Taper ratio.....0.3  
 Sweepback,  $0.25c$ ..... $45^\circ$   
 Airfoil section,  
 streamwise..... NACA 64A007

Wing area, total, sq ft..... 5.38

Tail area, total each plane,  
 sq ft.....1.35

Figure 1.- Principal dimensions and geometric characteristics of test models. All dimensions are in inches.

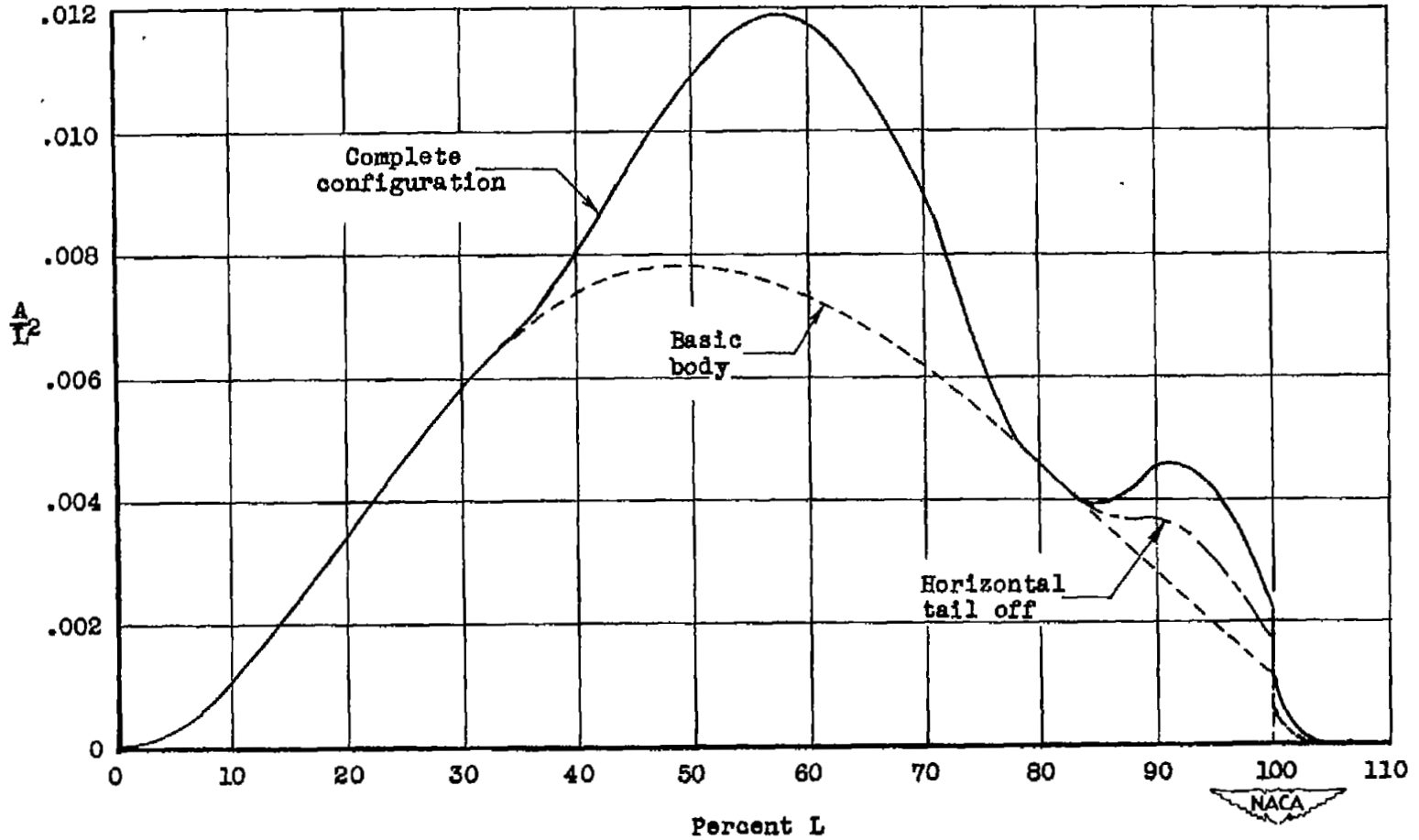


Figure 2.- Longitudinal distribution of cross-sectional area.

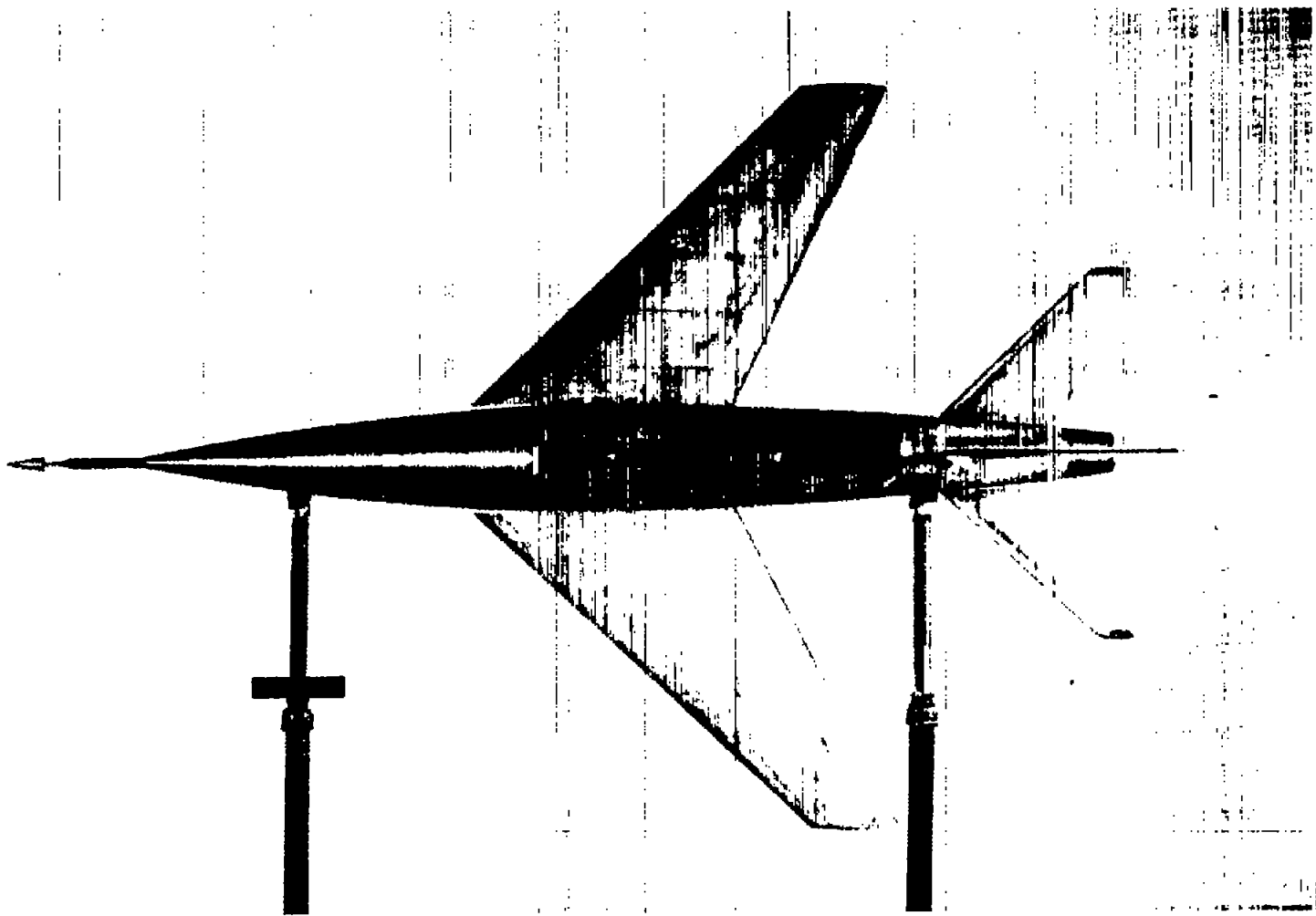
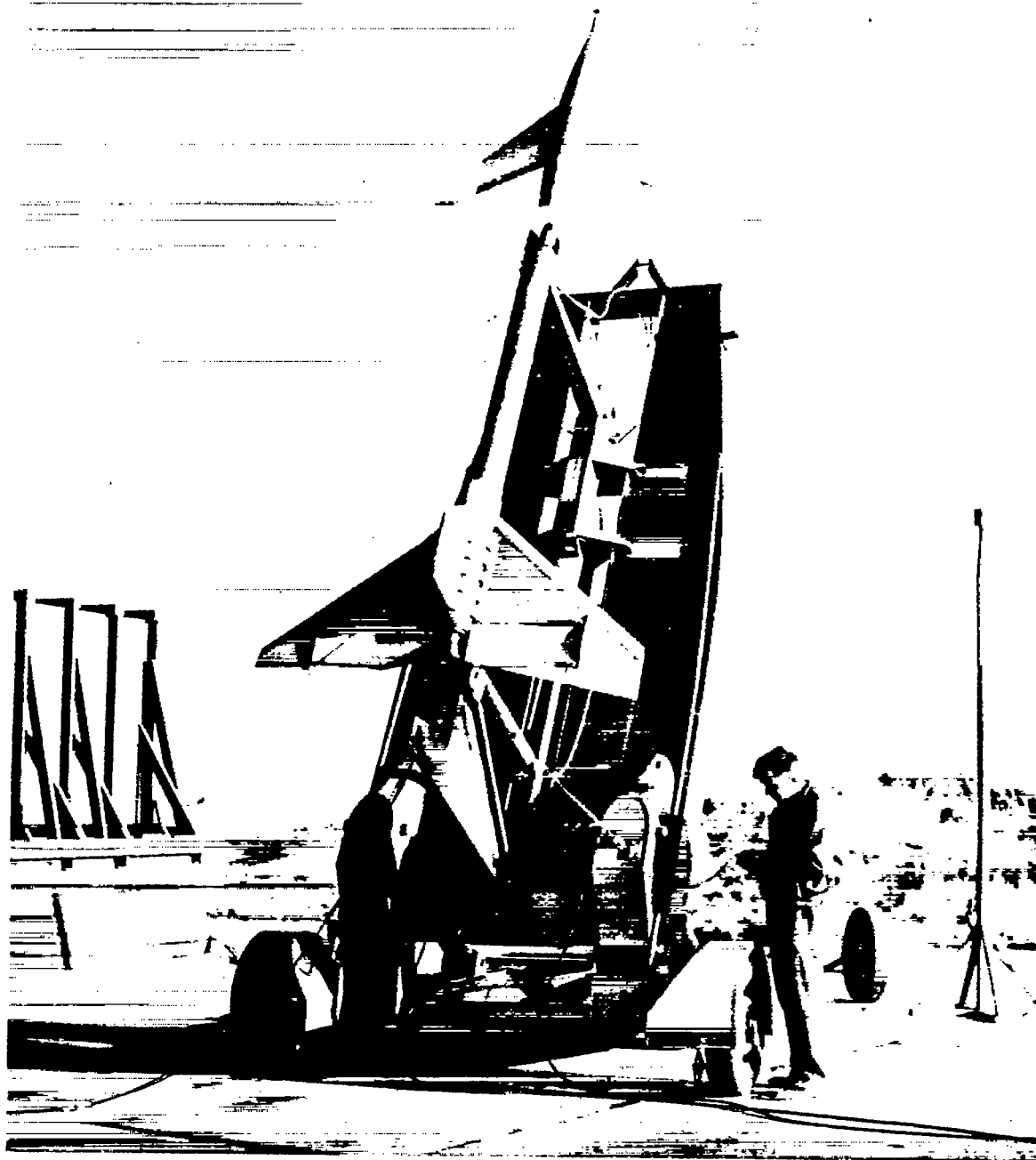


Figure 3.- Photograph of complete configuration.

L-76870.1



L-78389.1

Figure 4.- Photograph of tail-off model-booster combination on launcher.

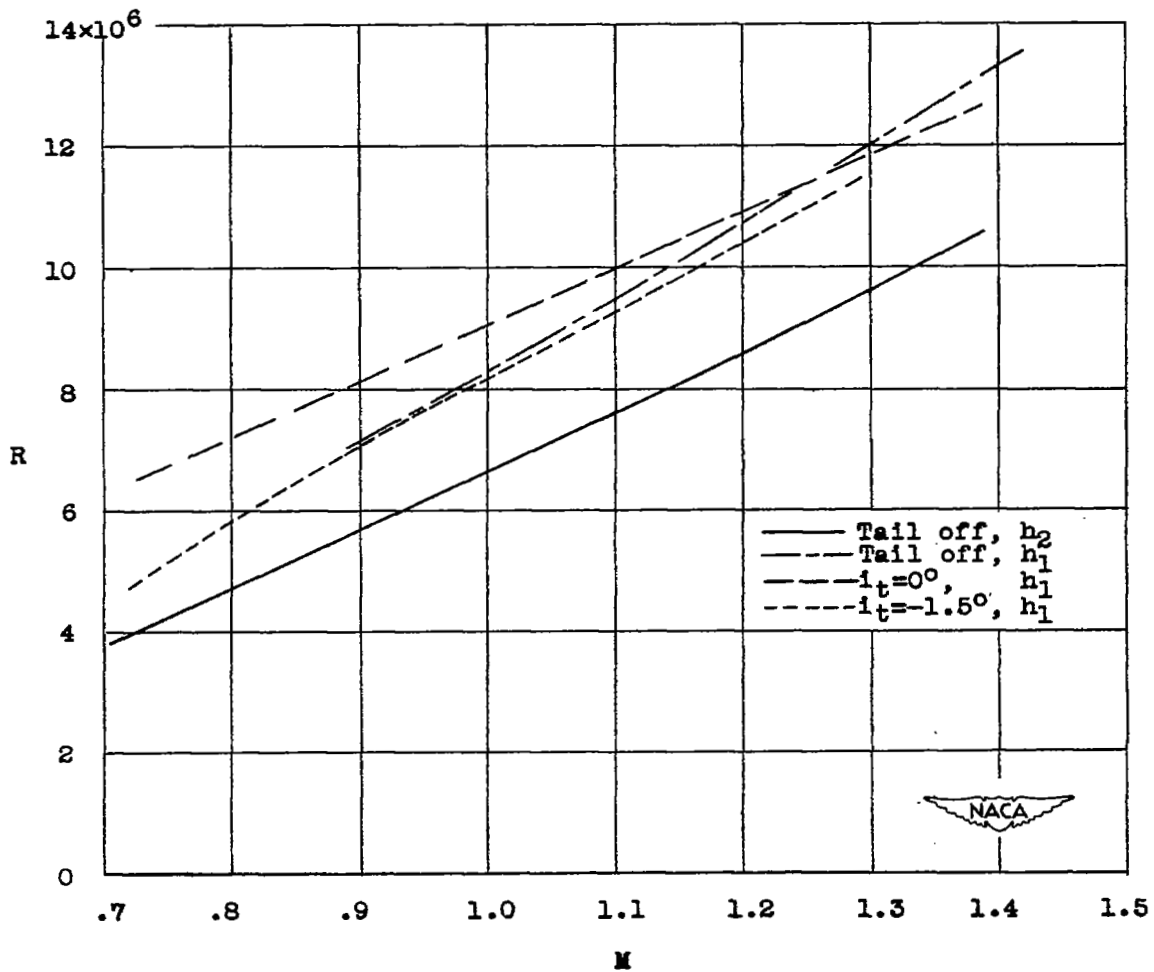


Figure 5.- Variation of Reynolds number, based on wing mean aerodynamic chord, with Mach number.

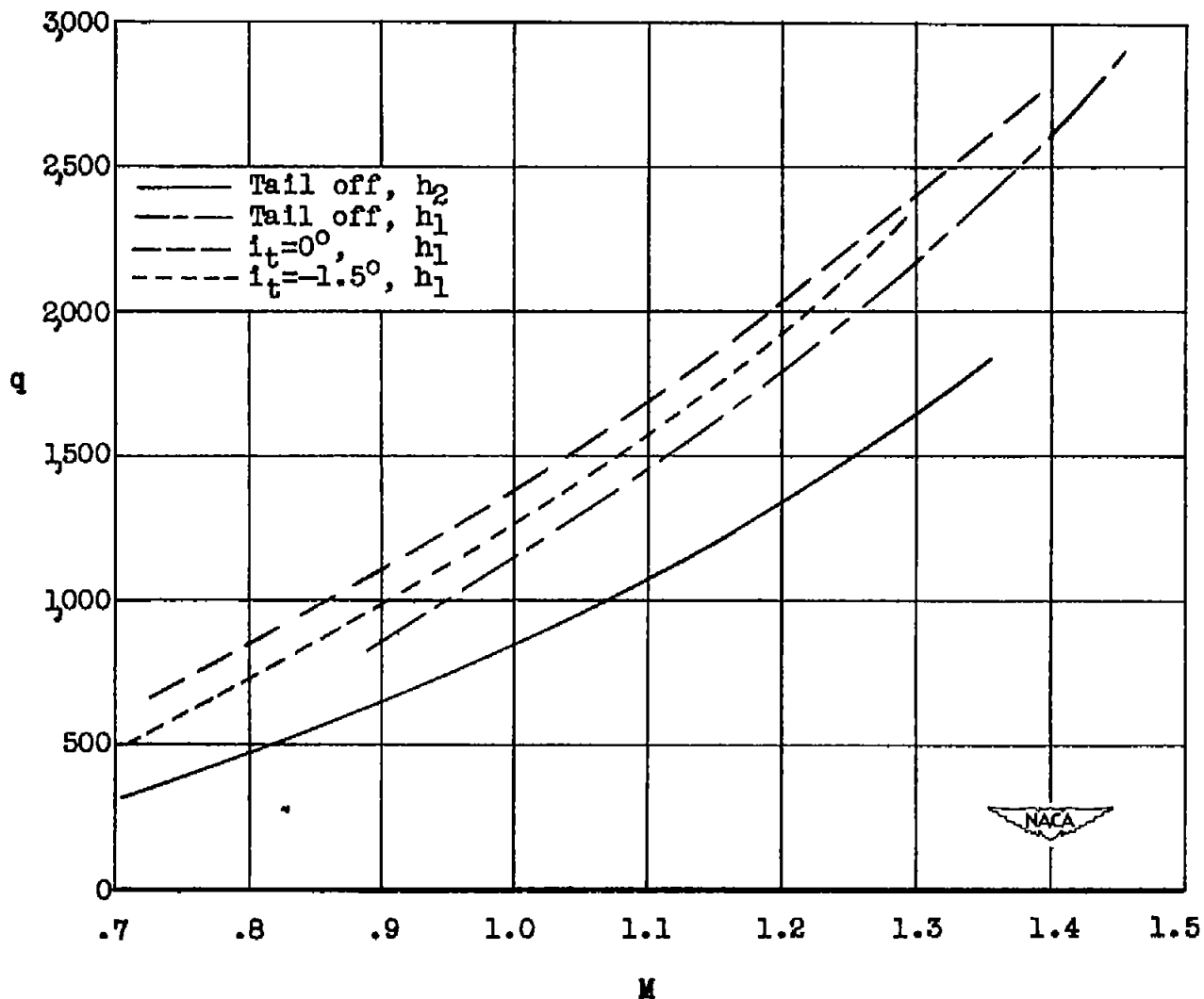


Figure 6.- Variation of free-stream dynamic pressure with Mach number.

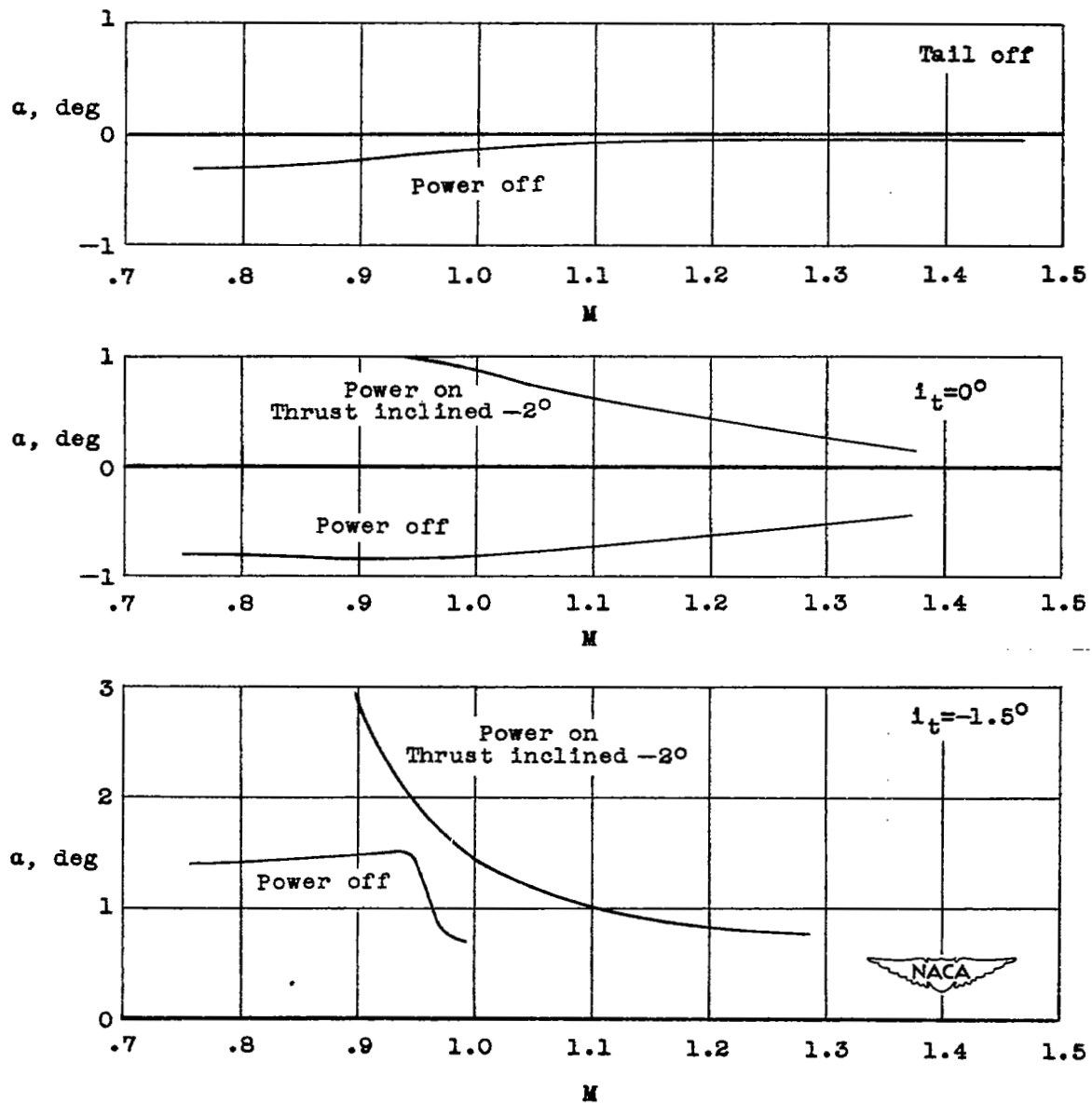


Figure 7.- Variation of trim angle of attack with Mach number.

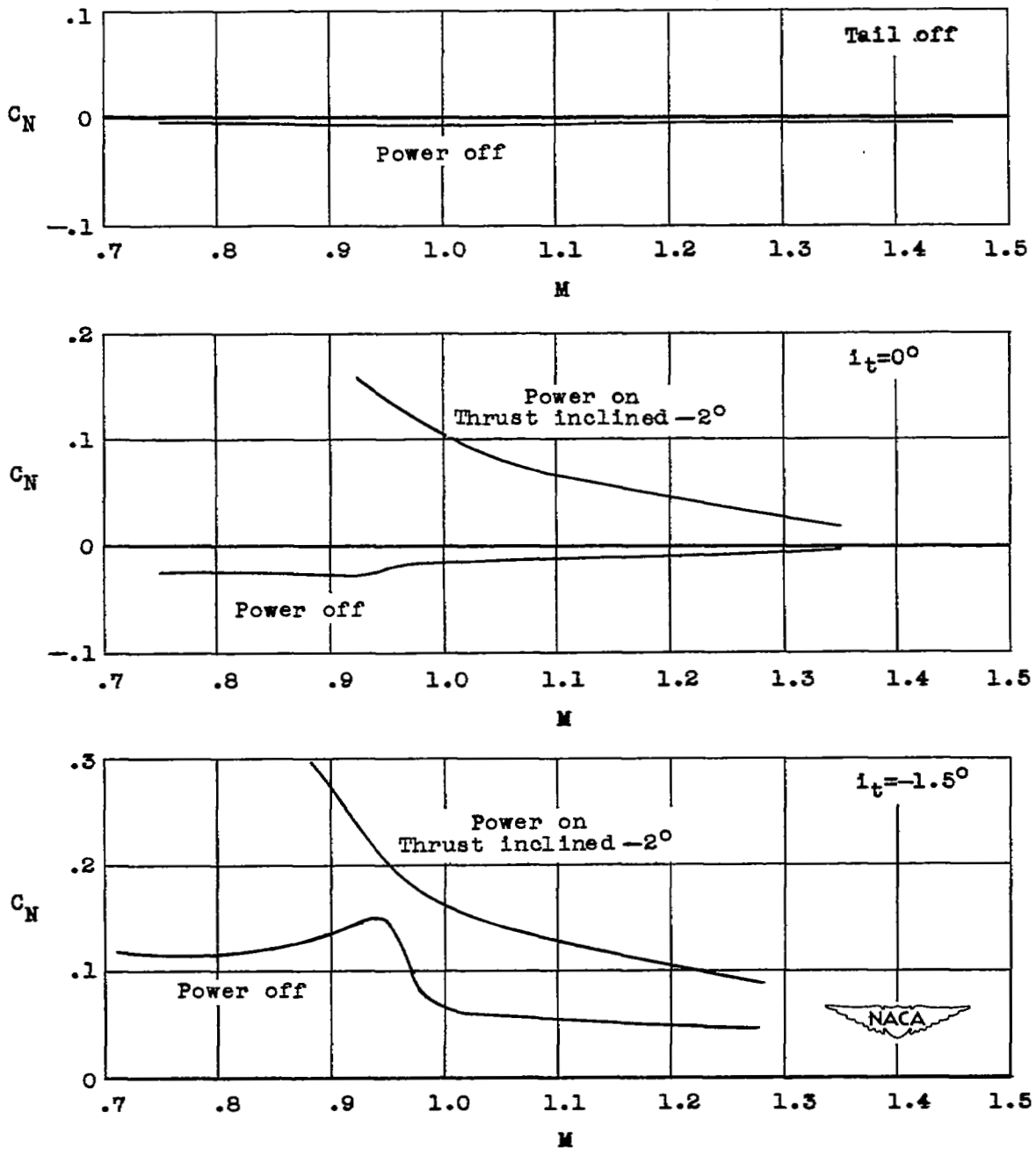


Figure 8.- Variation of trim normal-force coefficient with Mach number.

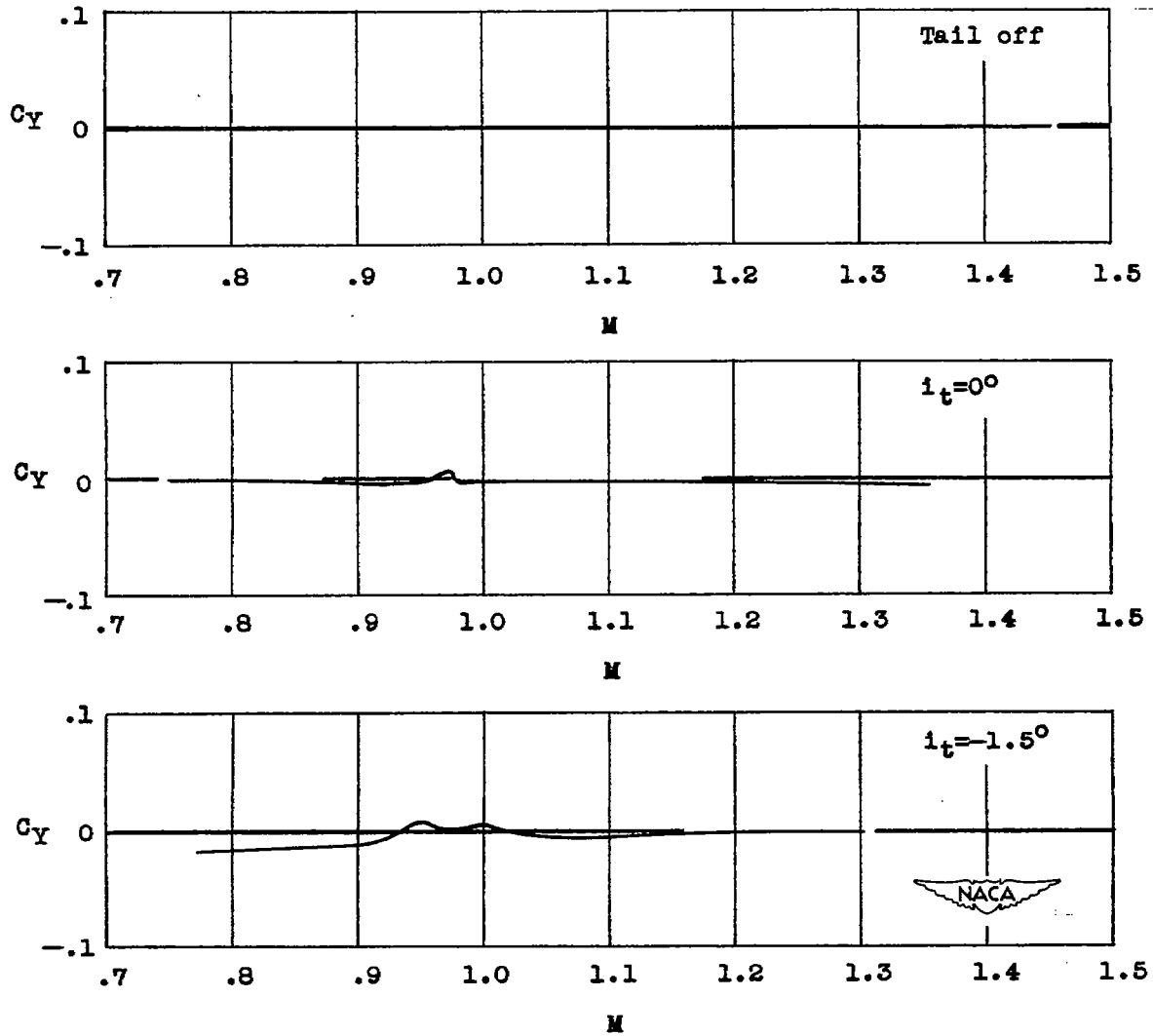


Figure 9.- Variation of trim side-force coefficient with Mach number during power-off flight.

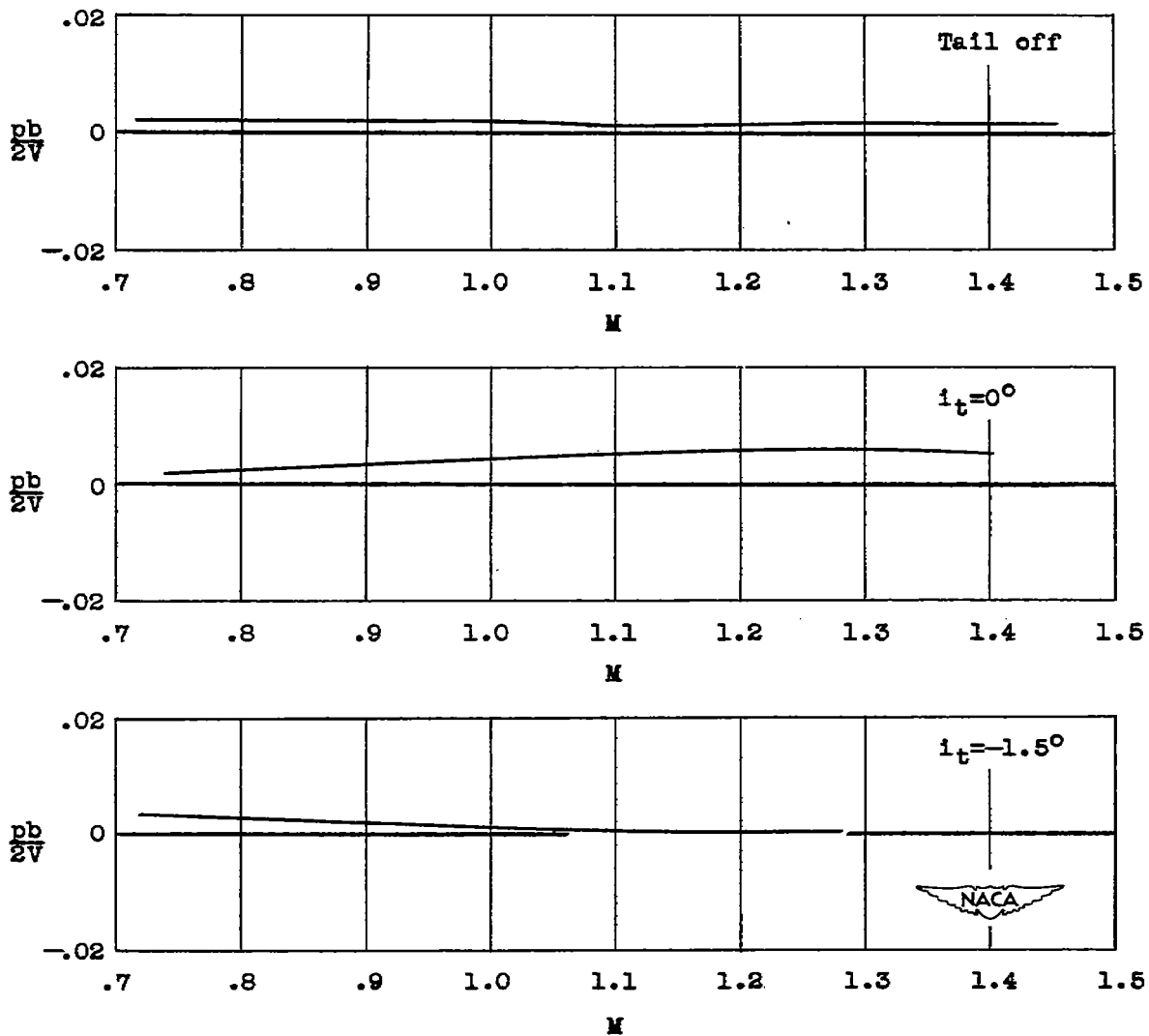


Figure 10.- Variation of wing-tip helix angle with Mach number during power-off flight.

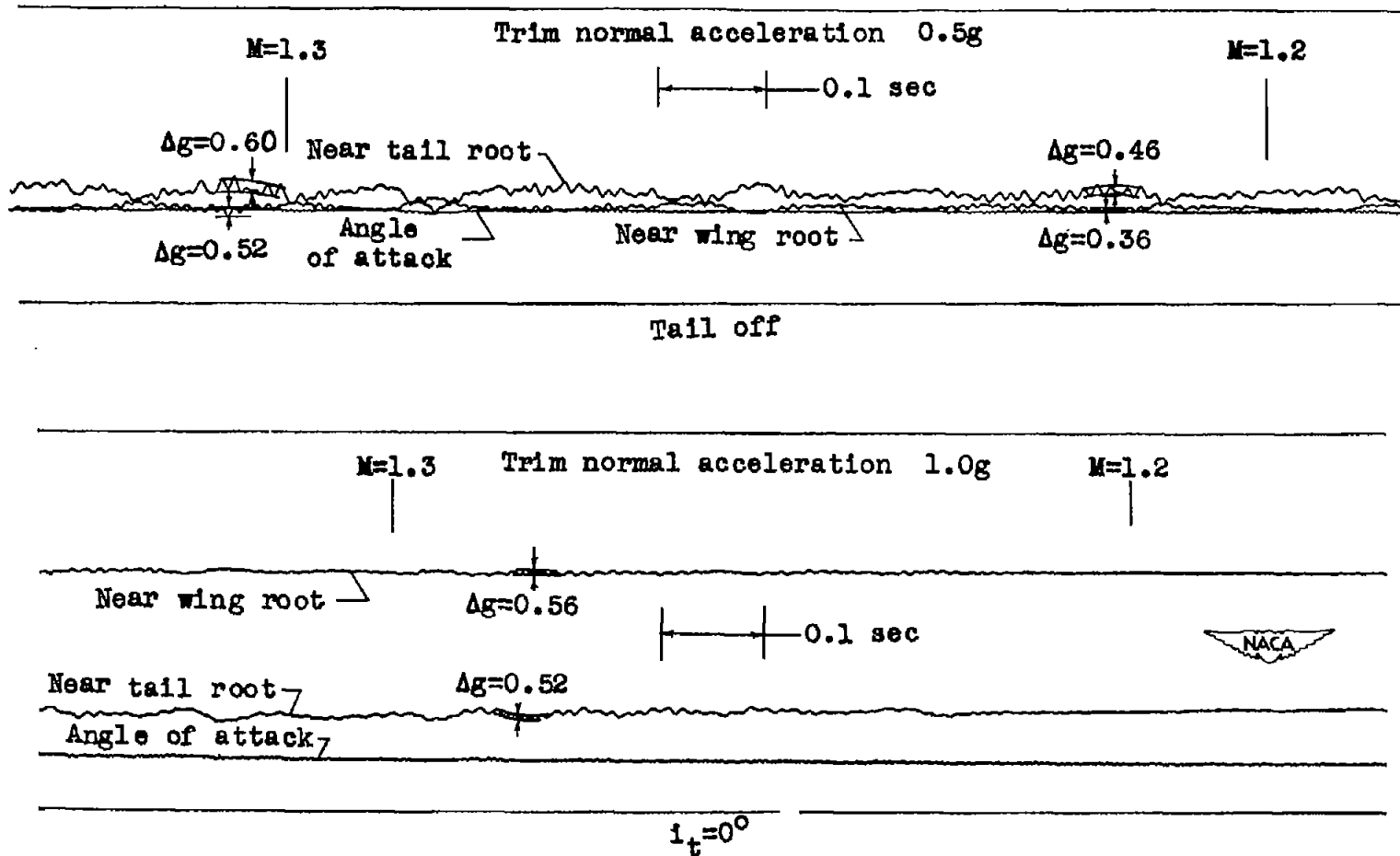


Figure 11.- Portions of telemeter records of normal acceleration during buffeting.

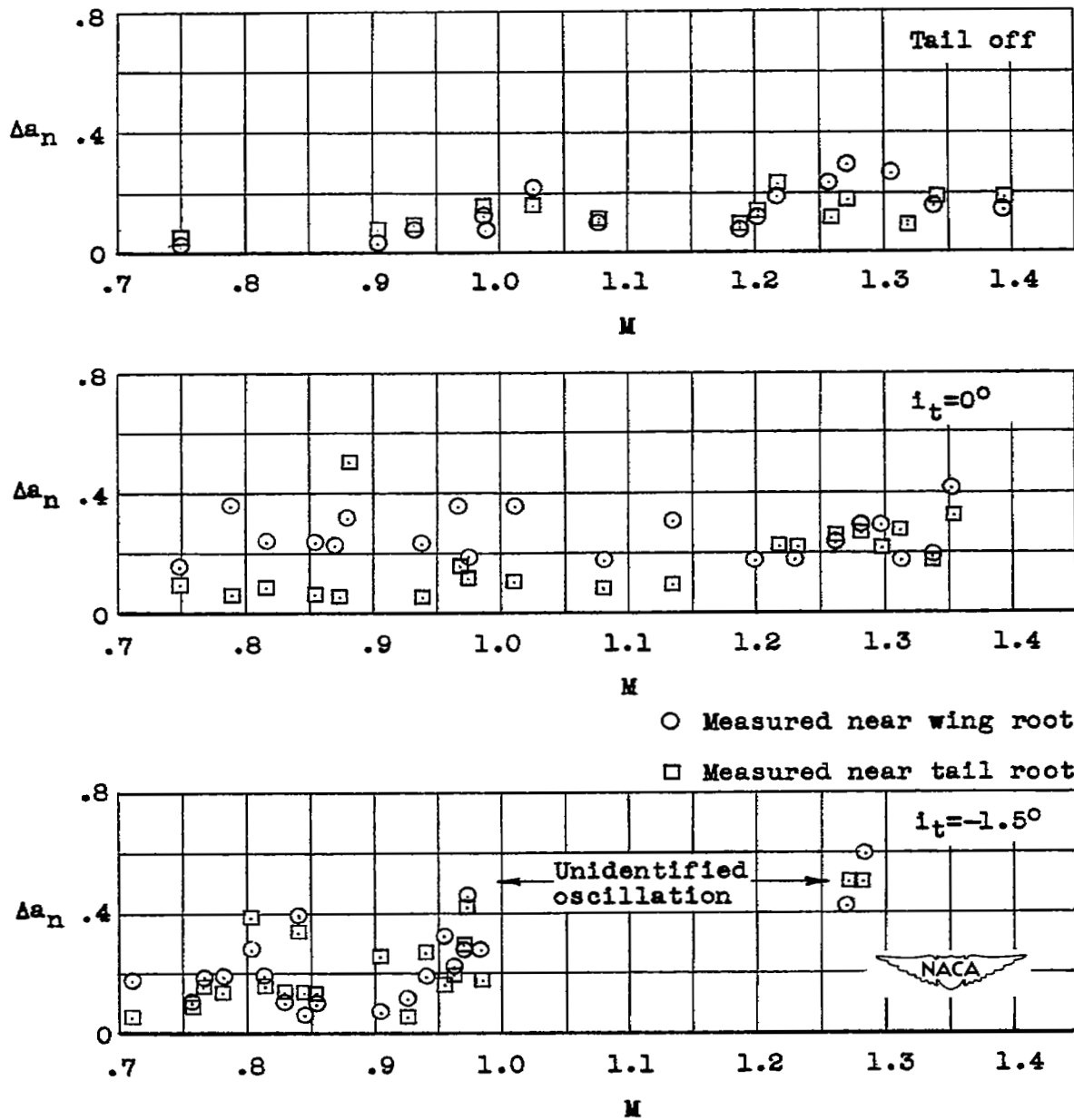


Figure 12.- Variation of normal buffet intensity with Mach number during power-off flight at a wing loading of approximately 20 lb/sq ft.

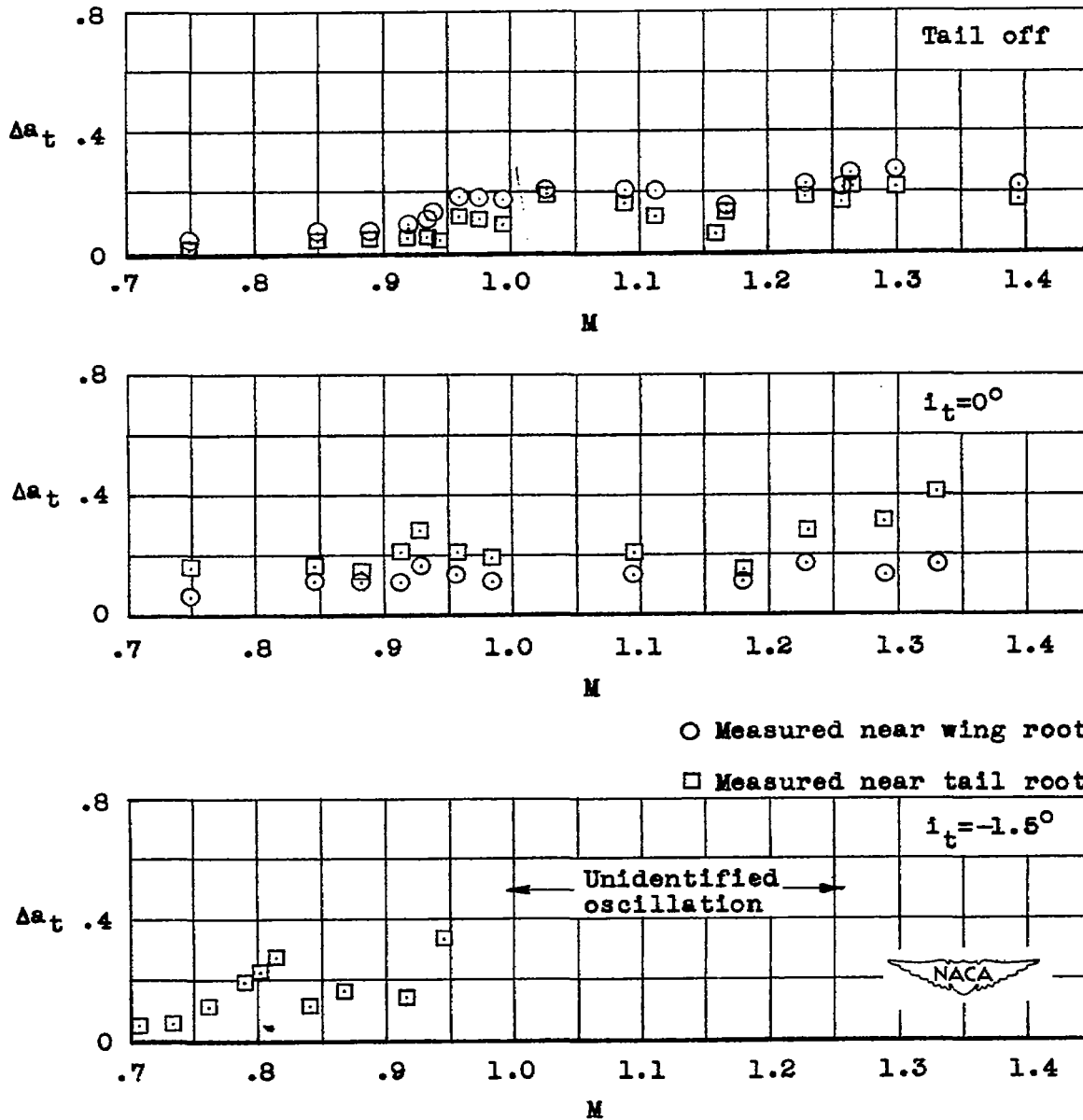


Figure 13.- Variation of transverse buffet intensity with Mach number during power-off flight.

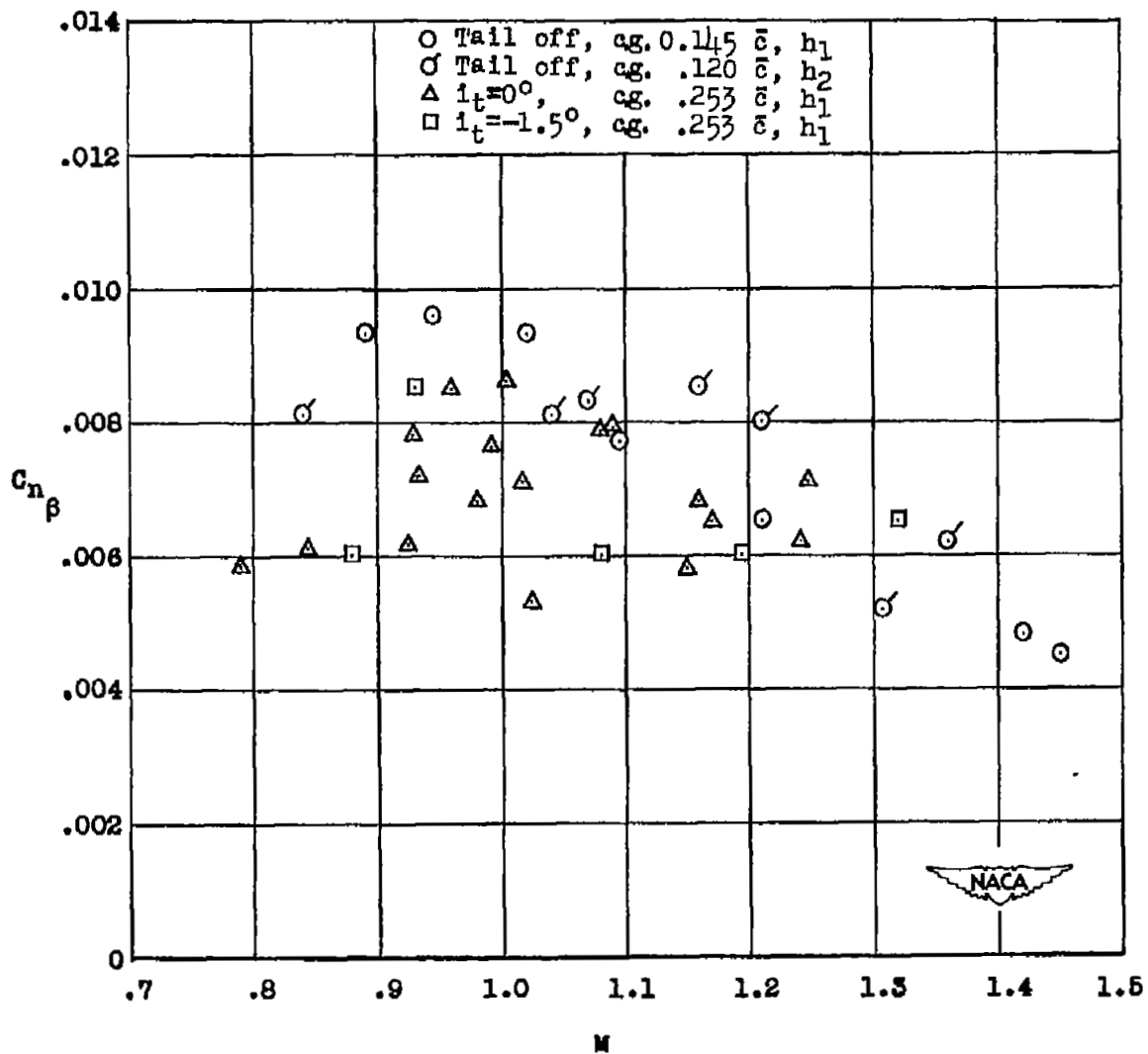


Figure 14.- Variation of static directional stability with Mach number during power-off flight.

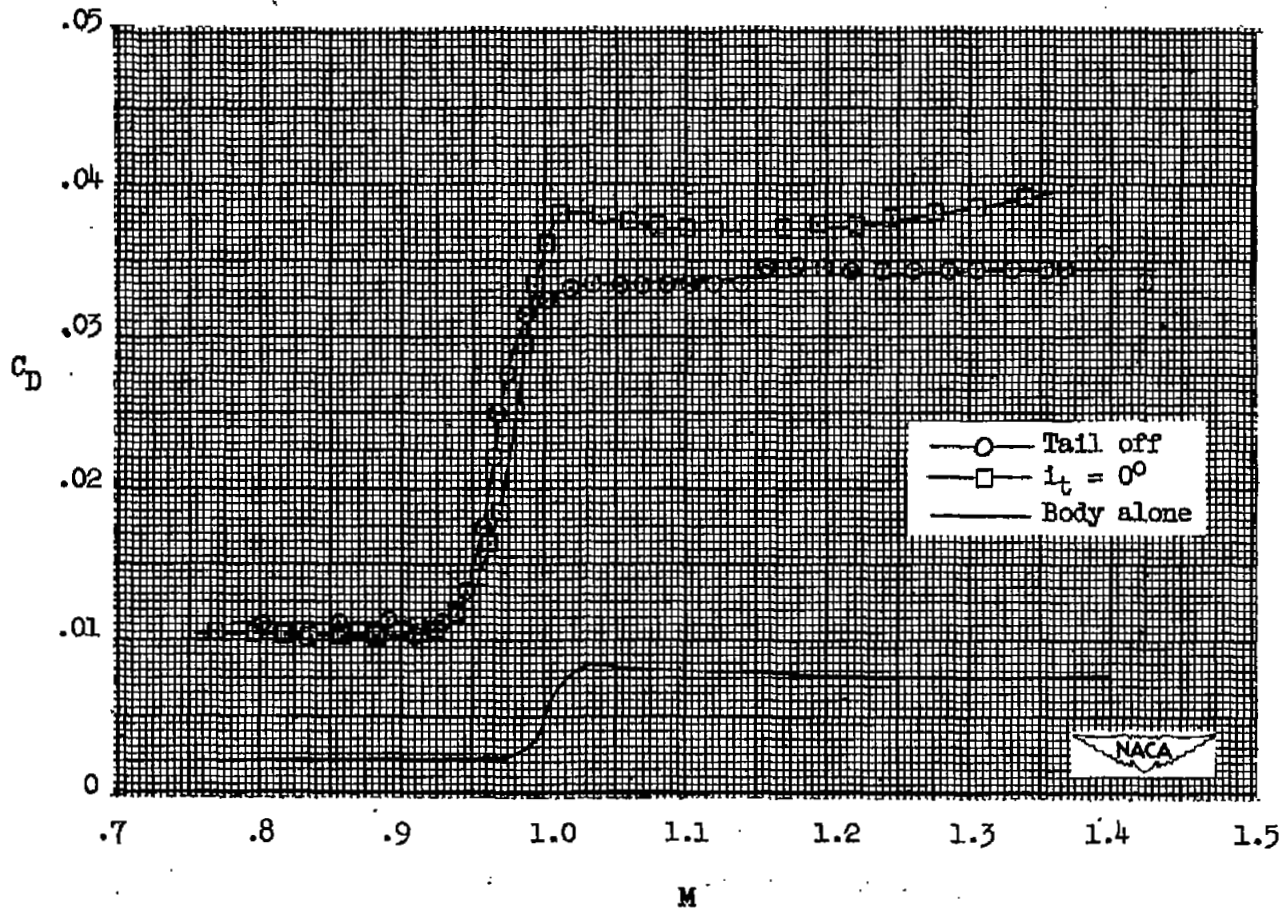


Figure 15.- Variation of drag coefficient, based on total wing area, with Mach number.

~~CONFIDENTIAL~~

ERRATA NO. 1

NACA RM L53110

FLIGHT TEST RESULTS OF ROCKET-PROPELLED BUFFET-RESEARCH  
MODELS HAVING  $45^\circ$  SWEEPBACK WINGS AND  $45^\circ$  SWEEPBACK  
TAILS LOCATED IN THE WING CHORD PLANE  
By Homer P. Mason

November 4, 1953

Page 26: Figure 15 should be replaced by the following revised figure 15.

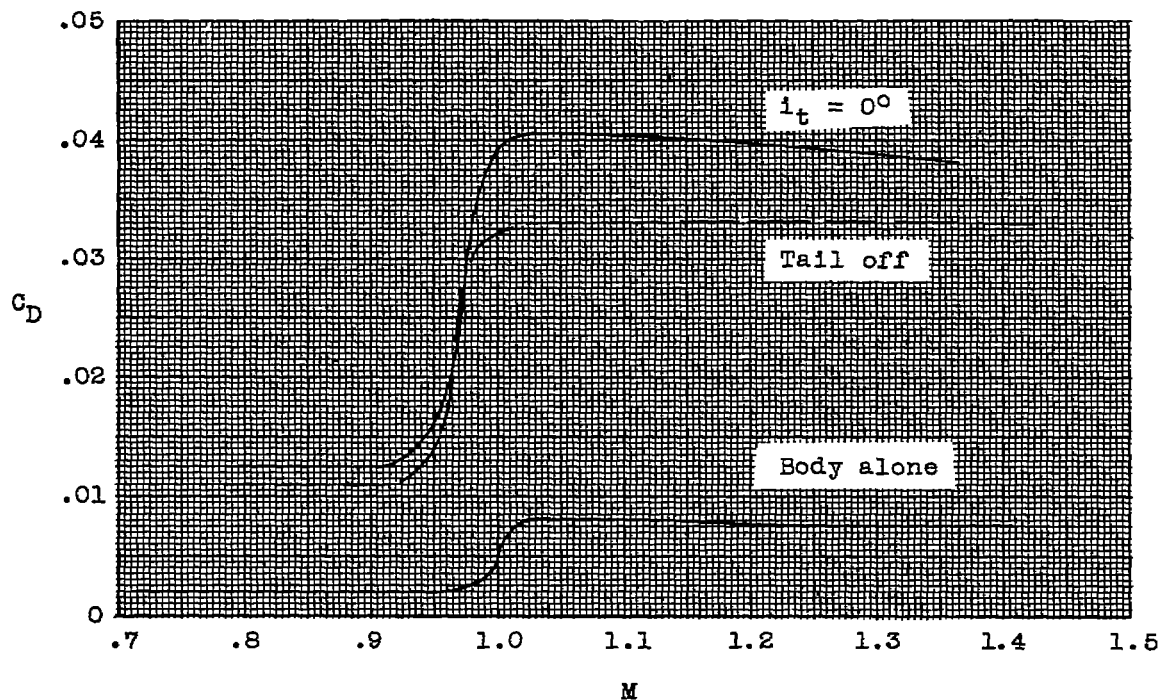


Figure 15.-Variation of drag coefficient, based on total wing area, with Mach number.

SECURITY INFORMATION



LANGLEY RESEARCH CENTER

3 1176 01345 5671

